Controlled Production of Molecule Corrals Using Cesium Ion Bombardment: A TOF−SIMS, XPS, and STM Study

Yingjie Zhu, Jennifer D. McBride, Terra A. Hansen, and Thomas P. Beebe, Jr.*

Department of Chemistry, Center for Biopolymers at Interfaces, and Surface Analysis Facility, University of Utah, Salt Lake City, Utah 84112

Received: October 31, 2000; In Final Form: January 4, 2001

The surface chemistry of highly oriented pyrolytic graphite (HOPG) bombarded with energetic Cs^+ ions was studied using the combined surface analysis techniques of TOF−SIMS (time-of-flight secondary ion mass spectrometry), XPS (X-ray photoelectron spectroscopy), and STM (scanning tunneling microscopy). Controlled surface modification of HOPG was achieved by bombardment of HOPG with Cs^+ ions at various energies ranging from 0.24 to 10 keV and at various dose densities. The experimental findings suggest that cesium implanted into HOPG exists in an oxidized state, i.e., in a form of cesium oxide. The Cs^+ bombardment of HOPG enhances oxygen adsorption due to both the dissociative adsorption of oxygen at HOPG defect sites produced by Cs^+ ions, and by the formation of cesium oxide. The surface coverage of cesium on HOPG increases linearly with increasing Cs^+ dose density at low bombardment energies ($\leq$ 1 keV) and is independent of Cs^+ dose density at high energies ($\geq$ 3 keV). The surface coverage of cesium decreases rapidly with increasing Cs^+ bombardment energy due to cesium implantation below the surface. The thermal stability of cesium in HOPG shows a complex behavior due to the competing effect of diffusion of cesium to, and desorption of cesium from, the HOPG surface at elevated temperatures. Defects in the HOPG created by the Cs^+ ion bombardment can subsequently be the starting sites for O_2 oxidation at elevated temperatures, producing "molecule corral" pits. The controlled pit production by the thermal oxidation on Cs^+ ion bombarded HOPG was realized and studied. The pit density, pit yield, and pit depth can be accurately controlled by varying Cs^+ dose density and bombardment energy. The defects induced by energetic ion bombardment of HOPG provide a promising method for the production of "molecule corrals" in the control of the pit density, pit spatial distribution, and pit depth. Controlled pit production on ion-bombarded HOPG has promising potential applications both scientifically and technologically.

Introduction

Highly oriented pyrolytic graphite (HOPG) is one of the most often studied substrates in surface science due to its unique properties. For example, it is atomically flat, easy to cleave, and relatively inert, even in air. It is also a weakly interacting substrate for STM and AFM (atomic force microscopy) molecular imaging and deposition experiments. Graphite is basically a two-dimensional solid, with strong covalent bonding in two-dimensional layers and only weak van der Waals interactions between the layers. Understanding the oxidative reaction of the basal plane of HOPG is both scientifically and technologically important because it is related to carbon combustion, coal gasification, reactions at nuclear reactor walls, removing carbon deposits from catalysts, and diamond thin-film growth. Pits on HOPG produced by the oxidation reaction have been developed as "molecule corrals" for the study of the ordering phenomena of self-assembled molecular monolayers in this group.[1] The molecule corrals have been used to confine molecule ensembles within small confined regions, and thereby they permit the analysis of molecular behavior by statistical methods and allow the measurement of several important properties that are difficult or impossible to determine by other techniques.[2−4] They also allow the observation of multiple independent molecular domains by STM.[5] The molecule corrals were also recently used as templates for the formation of metal and semiconductor nanostructures.[6−8]

The role of the surface defects in the formation of pits on HOPG has been well established in the literature.[1,9−15] These studies show that monolayer pits initiate from natural defects on the HOPG. Molecular oxygen dissociatively adsorbs at vacancy sites on graphite without an appreciable energy barrier.[16] Adsorbed atomic oxygen atoms react with carbon atoms on the graphite basal plane to form carbon oxides (CO or CO_2) that ultimately desorb into the gas phase. Multilayer pits have also been studied by STM, but they are normally observed so infrequently that only limited data could be obtained on them. A recent in-depth study by this group has allowed a direct comparison of monolayer and multilayer pit production under identical conditions.[15] Because the density of naturally occurring defects on HOPG is low, the density of pits formed by the oxidation reaction is also low. The pit depth and pit density are difficult to control because they are determined by the intrinsic nature and history of individual HOPG samples. Multilayer pits are especially difficult to produce because line defects that cut through many graphite layers are usually needed for the formation of pits with depths greater than two monolayers. Some multilayer pits observed by STM have been shown to also occur at screw defects,[15] which rarely occur on the HOPG surface.

* Corresponding author. Prof. Thomas P. Beebe, Jr., Department of Chemistry, HEB Room 3416, University of Utah, 315 South, 1400 East, Salt Lake City, UT 84112. Phone: 801-581-5383. Fax: 801-581-8433. E-mail: beebe@chem.utah.edu.

10.1021/jp0040300 CCC: $20.00
Published on Web 02/13/2001

Two methods have been used previously in an attempt to control pit density on the HOPG basal plane. The first was to use a lower grade of graphite,[15] ZYC as opposed to the higher grades of ZYA and ZYB. The lower grade of graphite contains a less ordered layering structure and more defects in the atomic stacking in the basal plane. The second method used to control pit density is to "thermally shock" the graphite during the oxidation process.[15,17] The thermal shocks did increase the pit density, but the amount of increase was highly variable and not reproducible.

A third method of controlling pit density, pit depth, and molecule corral production is the ion bombardment of HOPG. Ion bombardment of solid surfaces at ion energies above the threshold for penetration leads to inevitable changes in the atomic arrangement of the surface atoms. These changes, which are capable of modifying the structural, electrical, and chemical properties of the bombarded materials, have many technological applications in addition to being of scientific interest. Ion bombardment is an effective means for inducing new defects in a controlled fashion. Graphite has a layered structure and can accommodate guest species between its basal planes. This unique structure allows the projectile ions to become efficiently trapped and stabilized after surface penetration. Varying the ion dose density can control defect density, and subsequently control pit density. Bryant et al. first reported atomic-scale observation of defects on gold-deposited graphite by STM.[18] Later, two kinds of defects (vacancy and interstitial defects) caused by Ar^+ ion impact were reported.[19−25] The defects induced by the ion bombardment appeared as protrusions or hillocks of various sizes in STM images. Hillocks were proposed to originate from the enhanced charge density at the Fermi level of protrusion-like regions and may not have been actual topographic protrusions.[23]

Thermal oxidation of the ion-bombarded HOPG leads to the formation of size- and depth-controlled etch pits.[26−29] Hahn[26] reported thermal oxidation of graphite promoted by cesium interstitial defects by trapping cesium between the top two graphite sheets using 80 eV Cs^+ ion bombardment. Oxidation of HOPG bombarded by 80 eV Cs^+ ions at 650 °C led to the exclusive formation of monolayer pits. Hahn suggested that the pit formation started from cesium interstitial defects, which donated electron charge to the surrounding carbon atoms, promoting the upper layer to be reactive with O_2.

The surface chemistry and modification of HOPG bombarded with energetic ions plays a key role in graphite oxidation. Surface spectroscopic techniques can be employed for such studies. In this paper, TOF−SIMS, XPS, and STM were used to characterize HOPG surfaces bombarded with Cs^+ ions having an energy range from 0.24 to 10 keV. This paper will lead to a better understanding of what happens on the HOPG surface after Cs^+ bombardment and before thermal oxidation reactions, and it will help in the understanding of the formation mechanism of etch pits induced by thermal oxidation reactions on HOPG bombarded with energetic Cs^+ ions. Together these new insights will lead to an enhanced control of the production of nanometer-sized template features for numerous applications and fundamental studies.

Experimental Section

HOPG samples, grade ZYB, were generously supplied by Dr. Arthur W. Moore of Union Carbide/Advanced Ceramics. HOPG samples were cleaved with adhesive tape in ambient conditions. Immediately after cleaving, the HOPG samples were loaded into the TOF−SIMS ultrahigh vacuum (UHV) analysis chamber through the vacuum sample transfer system. The base pressure of the UHV analysis chamber was maintained at 10^{-10} mbar. The HOPG samples were bombarded with a Cs^+ ion beam generated from the Cs^+ ion gun of a TOF−SIMS instrument (TOF−SIMS IV, ION-TOF, Münster, Germany). The Cs^+ ion beam was rastered over a defined sample surface area for uniform ion exposure. TOF−SIMS measurements were performed by a 25 keV monoisotopic $^{69}Ga^+$ primary ion beam generated by a Ga^+ gun on the same TOF−SIMS instrument. "Bunched mode" was used to achieve highest mass resolution ($m/\Delta m \approx 10\,000$) in the mass spectra. The typical target current of the primary Ga^+ beam in the bunched mode for positive TOF−SIMS was 3 pA with a prebunched pulse width of 20 ns. The raster area of the Ga^+ ion gun was $500 \times 500\ \mu m^2$ and was adjusted to fall well within the area previously bombarded with the Cs^+ ion source. All primary Ga^+ ion fluences were below the damage threshold of 1×10^{13} ions cm^{-2} for static SIMS.

The Cs^+ ion bombarded HOPG samples were thermally oxidized by heating the samples at 650 °C (as measured by a chromel−alumel thermocouple) in a Lindberg Hevi-Duty tube furnace. The HOPG sample was placed in the center of a 2.5 cm × 60 cm horizontal quartz tube. Both ends of the tube were left open, and no effort was made to cause or prevent air flow.

XPS data were obtained using a VG ESCALAB 220i-XL electron spectrometer (VG Scientific Ltd., East Grinstead, UK). Monochromatic Al K_α X-rays (1486.7 eV) were employed. Typical operating conditions for the X-ray source were 400-μm nominal X-ray spot size (fwhm) operating at 15 kV, 8.9 mA and 120 W for both survey and high-resolution spectra. A 2-micron-thick aluminum window was used to isolate the X-ray chamber from the sample analysis chamber, to prevent high-energy electrons from impinging on the sample. Survey spectra, from 0 to 1200 eV binding energy, were collected at 100 eV pass energy with an energy resolution of ~1.0 eV, a dwell time of 100 ms per point, and a total of five scans averaged. High-resolution spectra were collected at a pass energy of 20 eV, energy resolution of ~0.1 eV, dwell time of 100 ms per data point, and a total of 20 scans averaged in the respective binding energy ranges. The C 1s peak, centered at 284.6 eV did not require charge shifting, therefore no charge shifting of other elemental peaks was employed. The data acquisition and data processing were done using Eclipse data system software. The operating pressure of the spectrometer was typically in the 10^{-9} mbar range with a system base pressure of 2×10^{-10} mbar.

The STM used in these studies is custom built and has been described elsewhere.[30] Typical scanning conditions used were: − 0.60 V (bias voltage), 160 pA (tunneling current). Images were acquired in constant-current (topographic) mode, using mechanically cut tips of 80% Pt/20% Ir. All images were acquired at room temperature under ambient conditions.

Results and Discussion

TOF−SIMS Spectra of HOPG. A positive-ion TOF−SIMS spectrum of HOPG cleaved by sticky tape was dominated by fragment ions $C_xH_y^+$. This contamination on HOPG most likely originated from adsorption of various components such as hydrocarbons from air although the HOPG samples were freshly cleaved. Note that the cleavage process was performed in the atmospheric environment followed by transfer to UHV immediately after cleaving. Metallic elemental ions such as Na^+, Mg^+, Si^+, K^+, and Ca^+ were found in the mass spectrum. Transition metallic ions such as V^+, Cr^+, Fe^+, Cu^+, and Zn^+ were not detected on the freshly cleaved HOPG surface but were detected on HOPG as received from the manufacturer. No C_{6n}^+

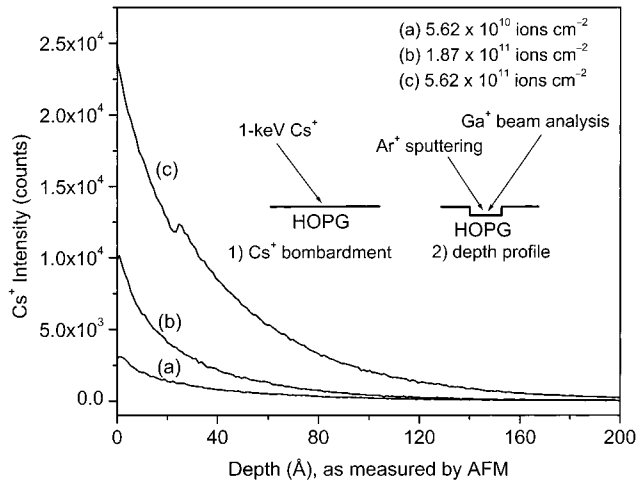

Figure 1. TOF−SIMS Cs^+ depth profiles on HOPG bombarded with 1 keV Cs^+ at various dose densities. (a) 5.62×10^{10} ions cm^{-2}; (b) 1.87×10^{11} ions cm^{-2}; (c) 5.62×10^{11} ions cm^{-2}. A 3 keV Ar^+ ion sputter gun was used (for sample erosion) in conjunction with a Ga^+ primary ion gun (for sample analysis) in order to examine the depth concentration profile of Cs^+ ions implanted in HOPG. The Ga^+ analysis beam was directed to the center of the sputter crater formed by the Ar^+ erosion gun. All above experiments were performed in UHV. All sputter crater depths were measured by ex-situ AFM in air.

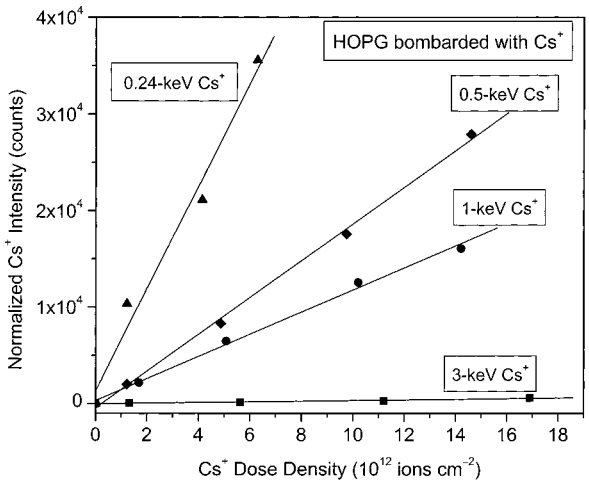

Figure 2. Normalized TOF−SIMS Cs^+ ion intensity on HOPG as a function of Cs^+ ion dose density at various Cs^+ bombardment energies: 0.24 keV Cs^+; 0.5 keV Cs^+; 1 keV Cs^+, and 3 keV Cs^+. HOPG samples were first bombarded with Cs^+ ions at various energies and at various Cs^+ ion dose densities. Then a Ga^+ primary ion gun was used in a "bunched mode" for sample analysis. All experiments were performed in UHV.

($n = 1, 2, 3$ ...) cluster ions were detected. Fragment ions $C_xH_y^-$ dominated the negative-ion TOF−SIMS spectrum of HOPG. O^-, OH^-, and F^- ions were also quite intense in the mass spectrum.

There was no Cs^+ ($m/z = 133$) peak in the positive-ion mass spectrum of freshly cleaved HOPG. However, an intense Cs^+ peak appeared after energetic Cs^+ bombardment of HOPG, indicating that Cs^+ ions were implanted into and at the HOPG surface by Cs^+ ion bombardment. This will be discussed in greater detail below.

Depth Profiles of Cs^+ Bombarded HOPG. The depth distribution of Cs^+ ions implanted into HOPG was studied by a TOF−SIMS depth profile, as shown in Figure 1. The HOPG samples were bombarded with 1 keV Cs^+ ions at different dose densities. Then a 3 keV Ar^+ ion sputter gun was used (for sample erosion) in conjunction with a Ga^+ primary ion gun (for sample analysis) in order to examine the depth concentration profile of Cs^+ ions implanted in the HOPG substrate. The Ga^+ analysis beam was directed to the center of the sputter crater formed by the Ar^+ erosion gun. All sputter crater depths were measured by ex-situ AFM to calibrate the sample erosion rate, which was assumed to be linear with time.

The lowest energy paths for surface penetration go through the center of a hexagonal carbon ring. Head-on collisions with carbon atoms require the highest energy for penetration.[31] Cs^+ ions, due to their heavier mass and larger size, penetrate through graphite layers at high energies regardless of their impact site. It becomes impossible for Cs^+ ions to cross a basal plane after they penetrate to a certain depth due to extensive kinetic energy losses. At the end of the trajectories Cs^+ ions settle between the graphite basal planes. Location of the final positions gives a depth distribution of cesium in HOPG. Cs^+ ions implanted into the HOPG exist as interstitial defects. The Cs^+ has a diameter of 3.38 Å which is almost the same as the spacing between the HOPG basal planes (3.35 Å). From a steric point of view, there should be some deformation of the graphite layers caused by cesium interstitial defects.

From Figure 1, one can see that the Cs^+ intensity below the surface decreases with the depth at an energy of 1 keV Cs^+ bombardment. The TOF−SIMS intensity of Cs^+ ions increases with the Cs^+ ion dose density (a, b, c) at a certain depth. For example, the intensity of Cs^+ ions is higher in curve c (0.015% of a ML Cs^+) than that in curve b (0.005% of a ML Cs^+) or curve a (0.0015% of a ML Cs^+) at the same depth. The ML units used above and throughout refer to exposures given in units of monolayers of carbon, regardless of the final surface coverage or penetration depth. Below we will discuss a cesium surface coverage on HOPG calibrated by XPS.

Cesium Surface Coverage. The defects on the HOPG surface induced by Cs^+ ion bombardment can be studied by STM. STM images of the HOPG surface bombarded with 1 keV Cs^+ ions without thermal oxidation show the randomly distributed hillocks that are defects induced by the Cs^+ ion bombardment. The hillocks were about 1−2.5 Å in height. Images similar to these obtained here have been reported in previous STM studies of graphite bombarded with other ions such as Ar^+ [19,20,23] and are not presented here. Such hillock-like features were not observed on the nonbombarded HOPG surface. The defects represented by hillock-like features in STM images may include both vacancy and Cs^+ interstitial defects.

The change in cesium surface coverage on HOPG as a function of the Cs^+ dose density was investigated using TOF−SIMS. The probe depth in static TOF−SIMS is limited to the topmost few atomic layers.[32] Therefore, TOF−SIMS gives useful information about cesium coverage at or near the surface. Figure 2 shows the TOF−SIMS Cs^+ ion intensity as a function of the Cs^+ dose density on the HOPG surface. A linear relationship exists between the measured Cs^+ ion intensity and the Cs^+ dose density at Cs^+ bombardment energies ranging from 0.24 to 3 keV. However, the slope of the fitted line, which represents the rate of change of the Cs^+ ion intensity with the Cs^+ dose density, varies for different Cs^+ bombardment energies. These slopes increase rapidly with decreasing Cs^+ bombardment energy. This implies that the Cs^+ concentration on the HOPG surface increases much faster with increasing Cs^+ dose density for lower Cs^+ bombardment energy than for higher Cs^+ bombardment energy. In essence, for a given Cs^+ dose density, more Cs^+ ions remain at or near the surface of the HOPG for lower energy Cs^+ ions than for higher energy Cs^+ ions. Higher energy Cs^+ ions penetrate deeper into the surface

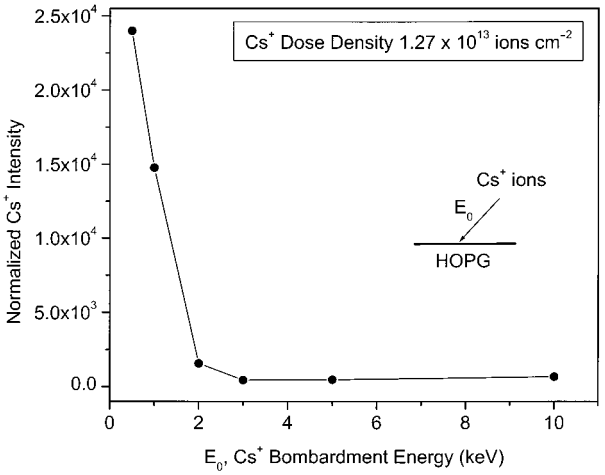

Figure 3. Normalized TOF−SIMS Cs^+ ion intensity on HOPG as a function of Cs^+ bombardment energy. HOPG samples were first bombarded with Cs^+ ions at various energies. The Cs^+ ion dose density is the same for all Cs^+ energies at 1.27×10^{13} ions cm^{-2}. Following this, a Ga^+ primary ion gun was used for TOF−SIMS analysis in UHV.

and therefore fewer Cs^+ ions are detected on the HOPG surface by TOF−SIMS. For bombardment energies higher than 3 keV, most of the Cs^+ ions penetrate into the HOPG, and almost no Cs^+ ions are left at or near the surface to be detected by the highly surface sensitive TOF−SIMS. This fact will be used below to control etch pit depth in molecule corral production.

The relationship between the surface Cs^+ intensity and the Cs^+ bombardment energy at a Cs^+ dose density of 1.27×10^{13} ions cm^{-2} is shown in Figure 3. The surface Cs^+ intensity decreases rapidly with increasing Cs^+ bombardment energy in the range from 0.24 to 2 keV. When the Cs^+ bombardment energy is higher than 3 keV, almost no Cs^+ ions are detectable by static TOF−SIMS on the HOPG surface because they are implanted at depths greater than the static TOF−SIMS sampling depth. Here it is interesting to mention the results reported by Choi et al.,[31] who studied the trapping of inert gas ions with lower energies (lower than 0.5 keV) at a higher dose density (10^{15}−10^{16} ions cm^{-2}) in HOPG. Their results showed that the concentration of trapped inert gas ions measured by AES (Auger electron spectroscopy) increased with increasing ion bombardment energy at very low energy range (lower than 0.1 keV). At a bombardment energy of more than 0.1 keV, the rate of increase in the concentration leveled off. In Choi's work, they used very low bombardment energy of inert gas ions that trapped within a few top graphite layers. The head-on backscattering upon collision with C atoms may play a role, and the penetration behavior is sensitive to the impact geometry and impact site in the low-energy range. The probing depth of AES is also deeper than for TOF−SIMS. All trapped inert gas atoms in HOPG bombarded with very low energy inert gas ions were likely detected by AES.

Control of Pit Depth. The TOF−SIMS results discussed above, in which higher energy Cs^+ ions penetrate deeper and create defects in the deeper graphite layers, are also supported by STM results, as shown in Figure 4. In this two-step experiment, defects for producing molecule corrals were first created by Cs^+ bombardment at different energies. These defects were then oxidized at an elevated temperature by O_2 to create molecule corrals for observation by STM. Figure 4a shows the pits formed on HOPG bombarded with 1 keV Cs^+ after oxidation at 650 °C for 7 min in air. Most of the pits were hexagonal in shape, and multilayer pits with depths from 2 to 6 monolayers were observed by STM. Deeper smaller pits that

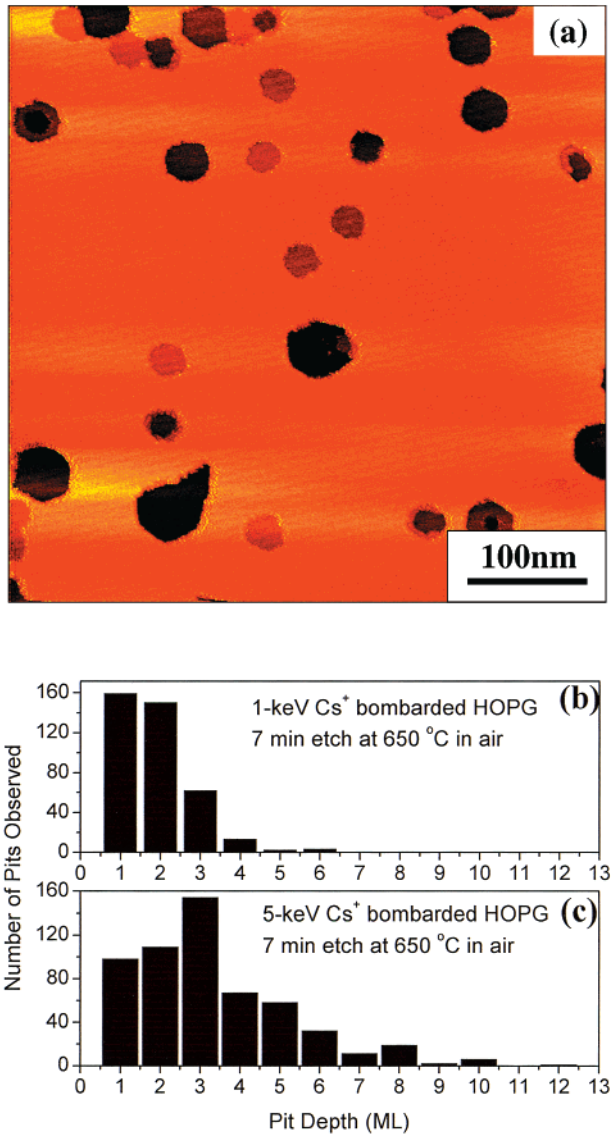

Figure 4. (a) Ex-situ STM image of HOPG bombarded with 1 keV Cs^+ in UHV at a dose density of 2.62×10^{10} ions cm^{-2}. The field of view is 500×500 nm^2 (b), and (c) the post-oxidation pit depth distribution measured by STM in air on HOPG bombarded with two different Cs^+ energies and subsequently etched at 650 °C in air for 7 min. (b) 1 keV Cs^+; (c) 5 keV Cs^+. Cs^+ dose density: 2.62×10^{10} ions cm^{-2} for both.

formed inside larger shallower pits were also observed. These results are in contrast with the results from Hahn,[26] who reported that circular pits with only monolayer depth were observed on low energy (80 eV) Cs^+ bombarded HOPG. This indicates that the ion bombardment energy has a significant effect on the depths of pits formed on HOPG.

The topographic and depth population profiles of defects, which are accessible to oxidation, can be examined by performing pit depth measurements (counting the numbers of pits with different depths) using STM. Figure 4b and 4c are a summary of STM statistical measurements on the pit depth distribution on HOPG bombarded with 1 keV and 5 keV Cs^+ ions. It demonstrates that the pit depth can be controlled by varying the Cs^+ ion bombardment energy. Multilayer pits originate from line defects that cut through many graphite layers caused by the penetrating energetic ions. Multilayer pits can be produced by Cs^+ ion bombardment at high enough energies. From Figure 4b, one can see that the deepest etch pits on HOPG bombarded with 1 keV Cs^+ ions are 6 monolayers in depth, and monolayer

TABLE 1: Effect of Cs^+ Dose Density on Pit Density and Pit Yield for HOPG Bombarded with 1 keV Cs^+

Cs^+ dose density (ions cm^{-2})	pit density (pits cm^{-2})	pit yield (pits per Cs^+ impact)
7.8×10^9	$(3.68 \pm 0.06) \times 10^9$	0.47 ± 0.02
2.6×10^{10}	$(1.29 \pm 0.06) \times 10^{10}$	0.49 ± 0.02
2.6×10^{11}	$(1.44 \pm 0.07) \times 10^{11}$	0.56 ± 0.03
5.6×10^{12}	$(4.64 \pm 0.23) \times 10^{11}$	0.083 ± 0.004

pits have the highest population percentage (40.87%). If the Cs^+ bombardment energy is increased to 5 keV, pits as deep as 12 monolayers form, and the highest population percentage (27.65%) pits are 3 monolayers deep (Figure 4c). This indicates that the higher energy Cs^+ ions penetrate deeper into HOPG and produce line defects that cut through more layers.

Control of Pit Density and Pit Yield. The pit density and thus pit yield (number of pits per incident Cs^+ ion) can be accurately controlled by varying the Cs^+ dose density, as shown in Table 1.

The pit density, usually intrinsically low on the unbombarded HOPG (from 1×10^8 to 2.5×10^9 pits cm^{-2}),[10,11,17] can be increased dramatically using Cs^+ bombardment. The pit density increases with increasing Cs^+ dose density. However, the pit yield changes in a different way. Pit yield, expressing the number of pits per incident Cs^+ ion, is essentially a measure of how efficiently pits are produced. The pit yield is almost constant at about 0.5 below a certain Cs^+ dose density and drops at higher Cs^+ dose densities, indicating that the efficiency of pit production decreases. However, the overall pit density continues to increase, but the rate of increase slows down at higher Cs^+ dose densities. These results can be explained in terms of damage area induced by each Cs^+ ion. At the low Cs^+ dose densities, the damaged areas are spaced apart from each other, and thus there is no overlap. Therefore, the defects induced by Cs^+ bombardment (and pit density) increase with increasing Cs^+ dose density, and the pit yield remains constant with increasing Cs^+ dose density. For a given Cs^+ ion dose density, 2.6×10^{11} ions cm^{-2}, rastered over a known graphite area and assuming a homogeneous Cs^+ ion distribution, the maximum graphite surface area per Cs^+ ion is calculated to be about 22 nm in diameter. If the Cs^+ dose density is much higher, the damaged areas will overlap with each other, decreasing the efficiency of defect production and thus the pit yield. There is also an effect of overlapping pit areas when the defect densities get high. This is an under-counting effect.

Cs^+ bombardment energy also has an effect on the pit density and thus pit yield, as shown in Figure 5. At a Cs^+ dose density of 2.62×10^{10} ions cm^{-2} corresponding to less than 10^{-5} ML, both the pit density and pit yield increase with increasing Cs^+ bombardment energy ranging from 0.3 to 10 keV. In the process of bombardment, Cs^+ ion energy is transferred to HOPG carbon atoms via atomic collisions, and a so-called collision cascade is generated. Part of the energy is transported back to the surface, allowing surface atoms to overcome the surface binding energy and subsequently to leave the surface and to produce defects on the surface. This phenomenon of energy transfer to the surface, and subsequent defect production, increases with increasing Cs^+ bombardment energy. It is therefore expected and observed that more defects are produced by bombardment with a higher Cs^+ energy at a fixed Cs^+ dose density. Defects that are effective for pit production may also include damaged surface areas without carbon atom vacancies. With higher Cs^+ bombardment energy, the surface damaged areas are expected to become larger. This may also make a contribution to an increase in pit density and pit yield.

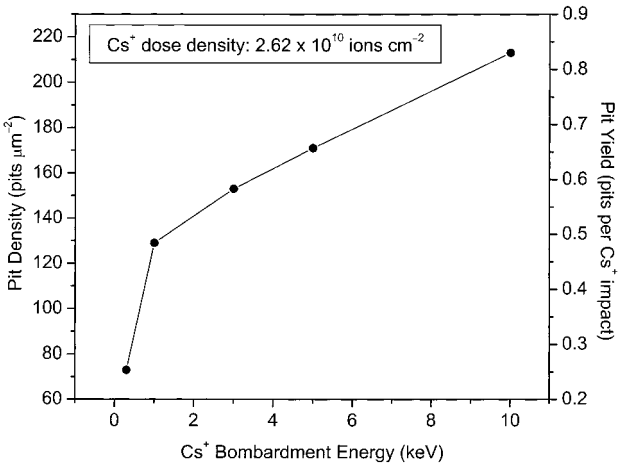

Figure 5. Pit density and pit yield as a function of Cs^+ bombardment energy at a Cs^+ dose density of 2.62×10^{10} ions cm^{-2}. Following generation of defects by Cs^+ ions, HOPG was oxidized at 650 °C in air for 7 min after Cs^+ bombardment in UHV.

XPS Analysis of Cesium and Oxygen on HOPG. XPS was used to quantify the surface coverage of cesium and oxygen and to study their respective chemical states. It is expected that the chemical state of Cs in HOPG plays an important role during the oxidation of HOPG. Hahn[26] suggested that the oxidation of graphite started from the cesium interstitial defects, which donated electron density to the surrounding carbon atoms, promoting the upper layer to be reactive with O_2 (the electron charge-transfer mechanism). No experimental evidence was available to determine the chemical state of cesium in Hahn's paper. Figure 6a shows the high-resolution Cs 3d XPS spectra of HOPG bombarded with 1 keV Cs^+ at a dose density of 2.43×10^{14} ions cm^{-2}. The Cs $3d_{5/2}$ peak is centered at 724.6 eV in comparison with a value of 726.4 eV for metallic Cs,[33] implying that Cs implanted into HOPG by Cs^+ bombardment is in an oxidized state in the form of a cesium oxide Cs_xO_y.

Adsorbed oxygen in HOPG plays a important role in the formation of pits. The presence of oxygen on the HOPG surface was studied by TOF−SIMS and XPS. In the negative-ion TOF−SIMS spectrum of HOPG, an intense O^- peak ($m/z = 16$) was observed. There was also an oxygen peak in the XPS survey spectrum of HOPG bombarded with Cs^+ ions in addition to cesium and carbon peaks. Figure 6b shows the high-resolution XPS O 1s spectrum. The intensity of the O 1s signal from the Cs^+ ion bombarded HOPG is considerably higher than that from an unbombarded control sample, indicating that Cs^+ ion bombardment enhances the oxygen adsorption on HOPG. This is supported by the following data, and we will provide an explanation later. The O 1s peak both from Cs^+ bombarded HOPG and the unbombarded control sample was fitted with two component peaks, as shown in Figure 6b. One component peak is located at 533.1 eV binding energy and is most likely due to the chemically adsorbed form of oxygen on HOPG. The second component peak is centered at a bonding energy of 531.9 eV, and is assigned to oxygen from oxygen-containing compounds. The peak intensity ratio (531.9 eV to 533.1 eV) is much higher for Cs^+ bombarded HOPG than that of the unbombarded control sample (∼2:1 versus 1:1). This may be due to the contribution of oxygen from cesium oxide in the Cs^+ bombarded sample.

The surface coverage of Cs on HOPG was quantitatively investigated by XPS. XPS probes the near-surface region with an exponentially decaying sampling depth of nominally 20 Å as estimated from the "universal curve" of the mean free path

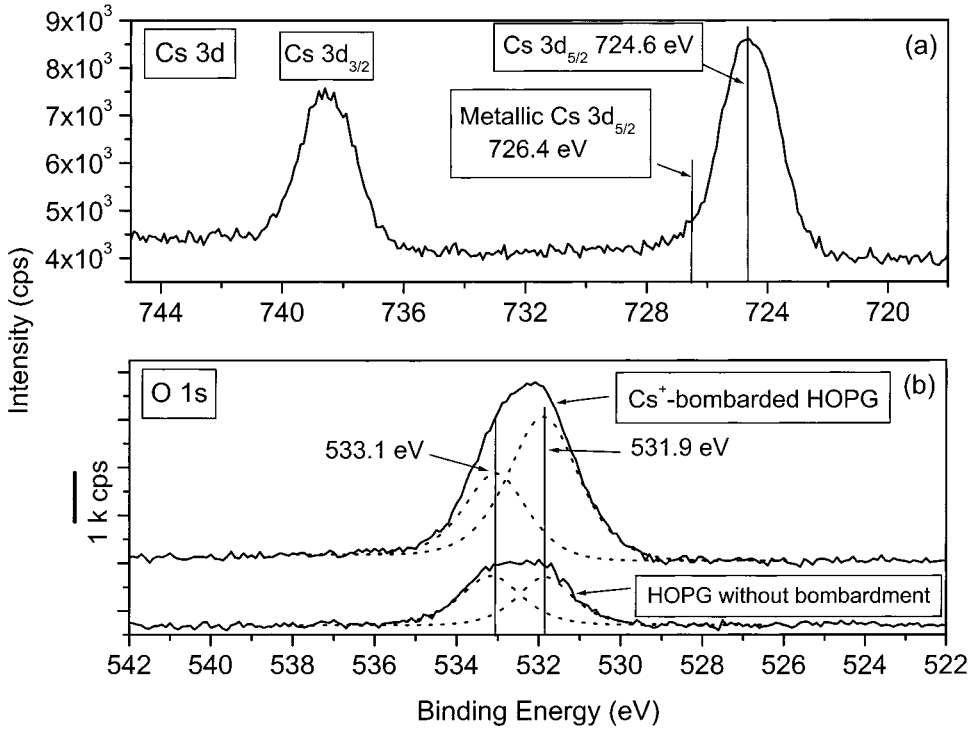

Figure 6. XPS high-resolution spectra of HOPG bombarded with 1 keV Cs^+ ions at a dose density of 2.43×10^{14} ions cm^{-2}. (a) Cs 3d; (b) O 1s. O1s spectrum of a control HOPG sample without Cs^+ bombardment is also shown.

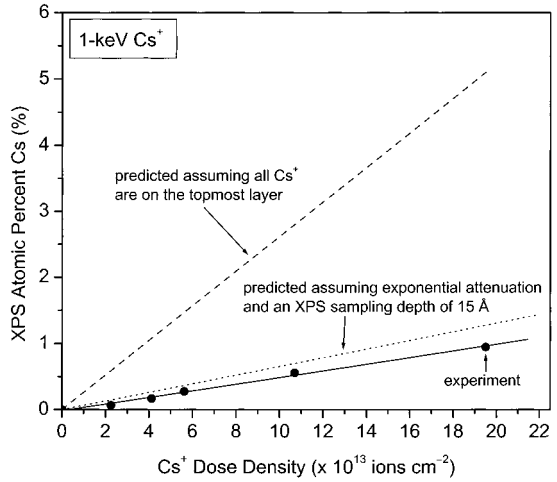

Figure 7. Atomic percent Cs on HOPG as a function of Cs^+ ion dose density for data measured by XPS. HOPG samples were first bombarded with 1 keV Cs^+ ions at various Cs^+ ion dose densities, then they were analyzed by XPS. See text for explanations of dashed curves.

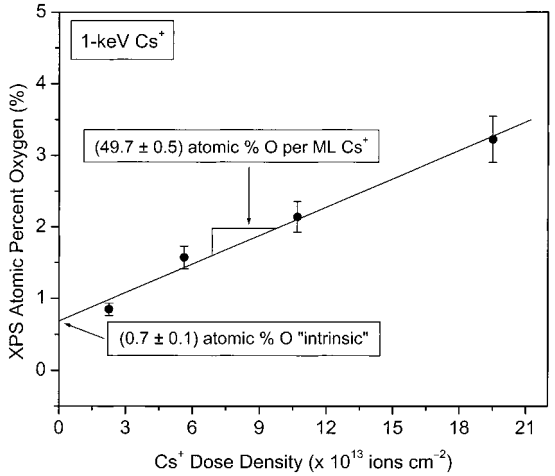

Figure 8. Atomic percent oxygen on HOPG bombarded with 1 keV Cs^+ measured by XPS as a function of Cs^+ ion dose density. HOPG samples were first bombarded with 1 keV Cs^+ ions at various Cs^+ ion dose densities, then they were analyzed by XPS.

of an electron with a kinetic energy of 1200 eV.[34] Figure 7 shows the results of the quantification of XPS spectral data for cesium on HOPG bombarded with 1 keV Cs^+ at various Cs^+ dose densities. The predicted cesium surface coverage, assuming unrealistically that all cesium is present on the topmost layer of HOPG, is also shown in Figure 7. As expected, the cesium coverage increases linearly with Cs^+ dose density, consistent with TOF−SIMS results shown in Figure 2. The predicted cesium coverage, assuming all cesium is on the topmost layer of HOPG, has a much higher slope than the experimentally determined line. Another predicted cesium coverage is also shown in Figure 7, assuming an exponential attenuation and a sampling depth of 15 Å. From Figure 4b it can be seen that essentially all cesium should be present in the upper 15 Å (4−5 layers deep) of the HOPG. The XPS sampling depth, and therefore the effective analysis volume, includes several of the top layers of carbon in addition to the Cs distributed among these layers. It is to be expected that the XPS-determined coverage is lower than the value calculated based upon a 1-monolayer model for two reasons. Some 1 keV Cs^+ ions become implanted at deeper levels where they experience attenuated sampling by XPS. Second, the total sampling volume includes several of the upper carbon layers, not only the first monolayer, thereby diluting the cesium concentration.

On the basis of the XPS measurements of the oxygen surface coverage, we found that Cs^+ ion bombardment of HOPG has an effect on the chemical adsorption of oxygen on the HOPG surface. Figure 8 shows atomic percent oxygen as a function of Cs^+ dose density. The oxygen surface coverage increases linearly with increasing Cs^+ dose density. This indicates that Cs^+ ion bombardment promotes the adsorption of oxygen on the HOPG surface. This can be interpreted in terms of

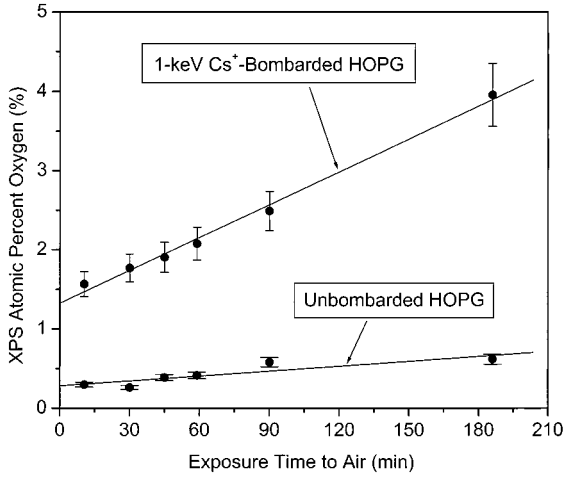

Figure 9. Atomic percent oxygen on HOPG as a function of exposure time to air for HOPG without Cs^+ ion bombardment and HOPG bombarded with 1 keV Cs^+ at a dose density of 2.43×10^{14} ions cm^{-2}. HOPG was cleaved by sticky tape in ambient conditions and immediately transferred into the UHV chamber for Cs^+ ion bombardment. Half of the HOPG sample was bombarded with Cs^+ ions and the other half of the sample was not bombarded as a control, and then the entire sample was exposed to air and subsequently analyzed by XPS.

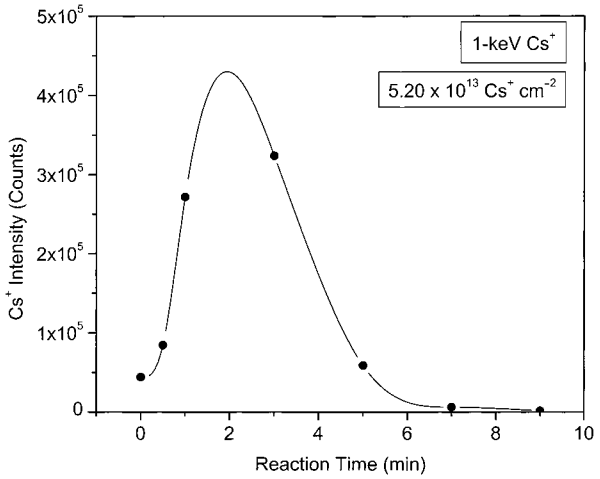

Figure 10. Normalized TOF−SIMS Cs^+ ion intensity on HOPG bombarded with 1 keV Cs^+ ions at a dose density of 5.2×10^{13} ions cm^{-2} as a function of reaction time at 650 °C in air. The HOPG sample was first bombarded with 1 keV Cs^+ ions in UHV and heated at 650 °C in air for various times and subsequently analyzed by TOF−SIMS in UHV.

dissociative chemisorption of O_2 at the carbon dangling bonds of vacancy defects induced by Cs^+ ion bombardment. There are reports[35−38] that adsorbed alkali metals enhance the adsorption and dissociation of O_2 by inducing various precursors. However, adsorbed metallic alkali metals, rather than implanted Cs^+ ions, were involved in these studies. It is very interesting to note that the fitted line does not go through the origin, and it is shown (Figure 6b) that unbombarded HOPG exhibits some oxygen adsorption. There is a positive *y*-intercept of (0.7 ± 0.1) atomic % oxygen, indicating an initial coverage of atomic oxygen "intrinsically" present on the HOPG surface prior to Cs^+ bombardment. The slope of the fitted line indicates the increased rate of oxygen coverage caused by the Cs^+ bombardment promotion effect. This slope was calculated to be (49.7 ± 0.5) % atomic oxygen per monolayer Cs^+. This means that, at least in this low-coverage range, one monolayer Cs^+ can cause the adsorption of 0.5 monolayer atomic oxygen on the HOPG surface. If we assume that all adsorbed oxygen caused by Cs^+ ion bombardment is due to cesium oxide, then the cesium oxide should have a chemical formula of Cs_2O in which cesium has an oxidation state of +1. If a fraction of this part of oxygen exists as atomic oxygen adsorbed at defect sites produced by Cs^+ bombardment, then the cesium oxide exists as Cs_xO_y, where $x/y < 2$.

Rates of O_2 Adsorption and Sticking Coefficients. Figure 9 shows the effect of 1 keV Cs^+ ion bombardment (Cs^+ dose density $= 2.43 \times 10^{14}$ ions cm^{-2}) on the surface coverage of oxygen as a function of exposure time to air. The time when the sample was taken out of the ultrahigh vacuum chamber was used as a starting point for the exposure time to air ($t = 0$). From Figure 9, one can see that the oxygen surface coverage on both unbombarded and Cs^+ bombarded HOPG increases with the exposure time to air, not surprisingly. However, the oxygen surface coverage on Cs^+ bombarded HOPG increases faster than that on the unbombarded HOPG, indicating that Cs^+ bombardment of HOPG has a promotion effect on oxygen adsorption onto the HOPG surface. On the basis of the slopes of both fitted lines in Figure 9, which represent the rate of increase of atomic oxygen on the HOPG surface, we calculated the O_2 molecule sticking coefficients on both the bombarded and unbombarded HOPG surfaces. The sticking coefficient is the ratio of the number of O_2 molecules adsorbed on the surface to the number of O_2 molecules that have collided with the surface. On 1 keV Cs^+ bombarded HOPG, the O_2 sticking coefficient is calculated to be $(1.02 \pm 0.08) \times 10^{-13}$ at 25 °C and an O_2 partial pressure of 0.16 atm. The O_2 sticking coefficient is $(1.53 \pm 0.35) \times 10^{-14}$ on the unbombarded HOPG surface under the same conditions.

The extremely low sticking coefficients for O_2 adsorption on HOPG are consistent with the widely known inertness of HOPG. It is important to point out that the sticking coefficient on defect sites is probably much higher than the 10^{-13} to 10^{-14} values reported here; the values reported here are averaged over all sites, the vast majority of which are perfect, defect-free carbon sites on HOPG. Cs^+ ion bombardment of HOPG may make two contributions to the promoted oxygen adsorption. One contribution is oxygen dissociatively adsorbed at defect sites produced by the Cs^+ bombardment. Another contribution is the formation of cesium oxide. The carbon vacancy defect sites and cesium interstitial defects may be two factors that contribute to the formation of pits on HOPG. The overall defect density on HOPG can be estimated from STM measurements of pit density, assuming that one defect produces one pit without considering an overlapping effect. From Table 1 one can see that the rate of increase in pit density levels off at higher Cs^+ dose densities. By extrapolation of these data, at a relatively high Cs^+ dose density of 2.43×10^{14} cm^{-2} (the ion dose density used in Figure 9), the pit density can be calculated to be on the order of 10^{12} pits cm^{-2}. It is difficult to experimentally measure such high pit densities with STM, because individual pits begin to overlap. If we consider only those O_2 molecules that collide with the defect sites (10^{12} sites cm^{-2}), then the O_2 molecule sticking coefficient is calculated to be on the order of 10^{-10}, 3 orders of magnitude larger than that averaged over all sites on the HOPG surface.

Thermal Stability of Implanted Cs^+ Ions in HOPG. The thermal stability of Cs^+ ions implanted in and on HOPG was studied by TOF−SIMS, as shown in Figure 10. The HOPG sample was bombarded with 1 keV Cs^+ ions at a dose density of 5.2×10^{13} ions cm^{-2}. Then the bombarded HOPG was reacted at 650 °C in air for different periods of time. TOF−SIMS was used to monitor the change of the Cs^+ ion intensity on the HOPG surface. It is surprising that at the early stage of

the reaction, the Cs^+ ion intensity increases (instead of decreasing) with reaction time up to 2−3 min. At 2−3 min reaction time, the Cs^+ ion intensity reaches its maximum, then decreases with the reaction time. After 7 min reaction time, the Cs^+ ion intensity decreases to almost zero.

According to the above experimental results, we propose that there are two processes that occur at an elevated temperature. One is a desorption process in which cesium leaves the HOPG surface. Another is an interplanar diffusion perpendicular to the graphite plane in which cesium atoms migrate up to the HOPG surface. These two processes occur simultaneously when the sample is held at an elevated temperature. Parallel diffusion of cesium between two basal planes may also play a role during the reaction. It is very likely that these cesium atoms find the defects in the upper basal plane and desorb through the defect holes. The pits, especially multilayer pits, expose the deeper basal planes, and we speculate that implanted cesium desorbs directly from the bottom of these pits without diffusion to the top graphite layer. At the early stage of reaction, the diffusion process dominates and more and more Cs atoms migrate to the surface, resulting in an increase in Cs^+ ion intensity. At 2−3 min of reaction time at 650 °C, the amount of Cs^+ diffused to the HOPG surface is maximized, leading to a maximum of Cs^+ ion intensity as measured by TOF−SIMS. After 2−3 min reaction time, the integrated effect of cesium desorption begins to dominate, leading to an overall decrease in the Cs^+ ion intensity on the HOPG surface. If the reaction time is long enough, all Cs^+ ions in HOPG are desorbed.

The migration of Cs^+ ions to, and their subsequent desorption from, the HOPG surface during the thermal oxidation undoubtedly plays a role in the formation of the pits. The enhanced adsorption of oxygen on HOPG induced by Cs^+ ion bombardment favors pit production. Additional studies of the formation of pits with controlled pit densities and pit depths for both Cs^+ and Ga^+ bombarded HOPG are in progress. These studies form a part of a larger set of studies designed to control the density, depth, size, and positions of molecule corrals for use as templates for the formation of nanostructures,[8] and as containers for studies of ensembles of isolated molecules.[1−5]

Conclusions

The surface modification of HOPG, resulting in controlled defect production and enhanced oxygen adsorption, was realized by Cs^+ ion bombardment. Defects in HOPG created by Cs^+ ion bombardment can subsequently be the starting sites for O_2 oxidation at elevated temperatures, producing "molecule corral" pits. The pit density, pit yield, and pit depth can be accurately controlled by varying Cs^+ dose density and bombardment energy. The surface coverage of cesium increases linearly with the Cs^+ ion dose density for Cs^+ bombardment energy $\leq$ 1 keV. Within this Cs^+ bombardment energy range, the cesium surface coverage decreases dramatically with increasing Cs^+ bombardment energy due to the fact that higher energy Cs^+ ions penetrate deeper into HOPG and fewer Cs^+ ions are left on the surface. For Cs^+ bombardment energies higher than 3-keV, the cesium *surface* coverage is almost independent of the Cs^+ dose density and the amount of cesium on the HOPG surface is almost negligible (Cs^+ ions are implanted at deeper levels beneath the surface). This is consistent with post-oxidation STM results of HOPG showing that deeper etch pits are formed on HOPG bombarded with a higher Cs^+ bombardment energy.

XPS results shows that cesium implanted in HOPG exists in an oxidized state (cesium oxide) rather than in a metallic state. The atomic percent oxygen increases linearly with increasing Cs^+ dose density because of the promoted oxygen adsorption on defect sites induced by Cs^+ ions and the formation of cesium oxide. The oxygen surface coverage increases linearly with the exposure time to air for both bombarded and unbombarded HOPG samples. However, the oxygen surface coverage on a Cs^+ bombarded HOPG surface increases faster than that on unbombarded HOPG, showing a promotion effect on oxygen adsorption by implanted Cs^+ ions, and oxygen adsorption on intrinsic defects. The thermal stability of implanted cesium on the HOPG surface shows a complex behavior at 650 °C in air because of the competing effects of Cs^+ ion diffusion up to, and subsequent desorption from, the HOPG surface.

Acknowledgment. Financial support from the National Science Foundation (CHE-9814477, DMR-9724307), the Alfred P. Sloan Foundation, and IPMI Student Award for Precious Metal Research (J.D.M.) is gratefully acknowledged. T.A.H. is an undergraduate scholar supported by the ACCESS program of the College of Science of the University of Utah. The authors thank Dr. Arthur Moore from Advanced Ceramics Corporation for his generous provision of HOPG samples.

References and Notes

(1) Patrick, D. L.; Cee, V. J.; Beebe, T. P., Jr. *Science* **1994**, *256*, 231−234.

(2) Patrick, D. L.; Cee, V. J.; Beebe, T. P., Jr. *J. Phys. Chem.* **1996**, *100*, 8478−8481.

(3) Schulze, J.; Stevens, F.; Beebe, T. P., Jr. *J. Phys. Chem. B*, **1998**, *102*(27), 5298−5302.

(4) Stevens, F.; Beebe, T. P., Jr. *Langmuir* **1999**, *15*(20), 6884−6889.

(5) Patrick, D. L.; Cee, V. J.; Morse, M. D.; Beebe, T. P., Jr. *J. Phys. Chem. B* **1999**, *103*(39), 8328−8336.

(6) Hövel, H.; Becker, Th.; Bettac, A.; Reihl, B.; Tschudy, M.; Williams, E. J. *J. Appl. Phys.* **1997**, *81*(1), 154−158.

(7) Hövel, H.; Becker, Th.; Bettac, A.; Reihl, B.; Tschudy, M.; Williams, E. J. *Appl. Surf. Sci.* **1997**, *115*, 124−127.

(8) McBride, J. D.; Van Tassell, B.; Jachmann, R. C.; Beebe, T. P., Jr. *J. Phys. Chem. B*, in press.

(9) Chang, H.; Bard, A. J. *J. Am. Chem. Soc.* **1990**, *112*, 4598−4599.

(10) Chu, X.; Schmidt, L. D. *Carbon* **1991**, 29, 1251−1255.

(11) Chu, X.; Schmidt, L. D. *Surf. Sci.* **1992**, *268*, 325−332.

(12) Tracz, A.; Wegner, G.; Rabe, J. P. *Langmuir* **1993**, *9*(11), 3033−3038.

(13) Tracz, A.; Kalachev, A. A.; Rabe, J. P. *Langmuir* **1995**, *11*(7), 2840−2842.

(14) Yang, R. T.; Wong, C. *Science* **1981**, *214*, 437−438.

(15) Stevens, F.; Kolodny, L. A.; Beebe, T. P., Jr. *J. Phys. Chem. B* **1998**, *102*, 10799−10804.

(16) Lee, S. M.; Lee, Y. H.; Hwang, Y. G.; Hahn, J. R.; Kang, H. *Phys. Rev. Lett.* **1999**, *82*(1), 217−220.

(17) Chang, H.; Bard, A. J. *J. Am. Chem. Soc.*, **1991**, *113*, 5588−5596.

(18) Bryant, A.; Smith, D. P. E.; Binning, G.; Harrison, W. A.; Quate, C. F. *Appl. Phys. Lett.* **1986**, *49*, 936−938.

(19) Hahn, J. R.; Kang, H. *Surf. Sci.* **1996**, *357−358*, 165−169.

(20) Marton, D.; Bu, H.; Boyd, K. J.; Todorov, S. S.; Al-Bayati, A. H.; Rabalais, J. W. *Surf. Sci.* **1995**, *326*, L489−493.

(21) Kang, H.; Park, K. H.; Kim, C.; Shim, B. S.; Kim, S.; Moon, D. W. *Nucl. Instrum. Methods B* **1992**, *67*(1−4), 312−315.

(22) Shedd, G. M.; Russell, P. E. *J. Vac. Sci. Technol.* **1991**, *A9*, 1261−1264.

(23) Hahn, J. R.; Kang, H.; Song, S.; Jeon, I. C. *Phys. Rev. B* **1996**, *53*(4), R1725−1728.

(24) Porte, L.; Phaner, M.; De Villeneuve, C. H.; Moncoffre, N.; Tousset, J. *Nucl. Instrum. Methods B* **1989**, *44*(1), 116−119.

(25) Li, T.; King, B. V.; MacDonald, R. J.; Cotterill, G. F.; O'Connor, D. J.; Yang, Q. *Surf. Sci.* **1994**, *312*(3), 399−410.

(26) Hahn, J. R. *Surf. Sci.* **1999**, *423*, L216-L221.

(27) Brauchle, G.; Richard-Schneider, S.; Illig, D.; Rockenberger, J.; Beck, R. D.; Kappes, M. M. *Appl. Phys. Lett.* **1995**, *67*(1), 52−54.

(28) Reimann, C. T.; Sullivan, P. A.; Türpitz, A.; Altmann, S.; Quist, A. P.; Bergman, A.; Oscarsson, S. O.; Sundqvist, B. U. R.; Hakansson, P. *Surf. Sci.* **1995**, *341*, L1019-L1024.

(29) Brauchle, G.; Richard-Schneider, S.; Illig, D.; Beck, R. D.; Schreiber, H.; Kappes, M. M. *Nucl. Instrum. Methods B* **1996**, *112*, 105−108.

(30) Zeglinski, D. M.; Ogletree, D. F.; Beebe, T. P., Jr.; Hwang, R. Q.; Somorjai, G. A.; Salmeron, M. B. *Rev. Sci. Instrum.* **1990**, *61*, 3769−3774.

(31) Choi, W.; Kim, C.; Kang, H. *Surf. Sci.* **1993**, *281*, 323−335.

(32) Benninghoven, A. *Angew. Chem., Int. Ed. Engl.* **1994**, *33*, 1023−1043.

(33) Moulder, J. F.; Stickle, W. F.; Sobol, P. E.; Bomben, K. D. *Handbook of X-ray Photoelectron Spectroscopy*; Chastain, J., King, R. C., Jr., Eds.; Physical Electronics, Inc.: Eden Prairie, Minnesota, 1995.

(34) Somarjai, G. A. *Chemistry in Two Dimensions*; Cornell University Press: Ithaca, NY, 1981.

(35) Sojval, P.; Kasemo, B. *J. Chem. Phys.* **1993**, *98*, 5932−5937.

(36) Chakarov, D. V.; Sojval, P.; Kasemo, B. *J. Phys. Condens. Matter* **1993**, *5*, 2903−2912.

(37) Janiak, C.; Hoffmann, R.; Sojval, P.; Kasemo, B. *Langmuir* **1993**, *9*, 3427−3440.

(38) Lamoen, D.; Persson, B. N. J. *J. Chem. Phys.* **1998**, *108*, 3332−3341.